Data Repository Item: Receiver functions, phase stacking, and tomography cross-sections

DR.1. Receiver functions

200 s, three-component seismograms are collected for all events with magnitude > 5.5 in the epicentral distance range 30-100°. The vertical and horizontal (radial and transverse) components of motion are decomposed into up-going P, SV (radial), and SH (transverse) wave components using the free-surface transfer matrix (Bostock, 1998). We retain seismograms with P-component signal-to-noise ratios > 10 dB of the first 10 seconds in the 0-2 Hz frequency band. Recorded events come mainly from the Western Pacific, Fiji-Tonga, and Central and South American regions. Back-azimuthal coverage is good from 225° to 360° and from 125° to 175°, and less regularly sampled otherwise. Because the strike of Cascadia subduction is approximately NW-SE, slab structure is sampled mostly from the updip and strike parallel directions.

Individual single-event seismograms are processed using the receiver function method, which uses the P component as an estimate of the source to deconvolve the SV and SH components and recover the receiver-side S scattering structure. This procedure is performed using a Wiener spectral deconvolution (Bostock, 1998). The resulting SV and SH receiver function time series represent forward (Pxs) and back-scattered (Ppxs, Psxs) waves from discontinuities in physical properties, identified by x (Figure DR1). The timing and amplitude of each converted phase constrain overlying velocity structure (depth and Vp/Vs of the overlying column) and velocity contrast, respectively.

To visualize coherent structural signals beneath individual stations we sort receiver functions by back-azimuth of incoming wavefield and display the time series as adjacent blue-red color-coded traces (Figure DR2). Amplitudes are relative to incident P-wave. These data are sensitive to structures with scale lengths of 1-10 km and are dominated by the signature of an eastward dipping low-velocity zone (LVZ). This signature includes 3 sets of oppositely polarized pulses comprising forward scattered Pxs conversions, and back-scattered Ppxs and Psxs conversions from the top (x=t) and bottom (x=b) of the LVZ.

DR.2. Phase stacking

The stacking technique is based on the work by (Zhu and Kanamori, 2001) for horizontal layering, and later adapted by (Rossi et al., 2006) for planar dipping layers. The procedure is based on stacking moveout-corrected traces for each weighted radial and transverse converted phase (Pxs, Ppxs, Psxs) in the receiver functions for a given model, and searching through a range of parameters. Because the moveout depends on the propagation path through the model for a given incident wavefield, all data at a given station can be used simultaneously. By stacking forward and back-scattered phases with different moveout curves, the stacks will interfere constructively and produce a maximum at the correct model.

This procedure is effective for simple layering and isotropic velocity structure. If anisotropy is present, the periodic back-azimuthal response of converted phases can in practice be corrected to account for polarity reversals, which would otherwise produce destructive interference in the stacks and thus bias the results (Figure DR3). Alternatively, one can carefully select phases that are less affected by anisotropy, for example by applying larger relative weight to those phases, in order to avoid this effect.

Strike direction along the margin is constrained by polarity reversals on transverse-component receiver functions (Figure DR2, DR3). We use the phase-weighted stacking technique of Schimmel and Paulssen, (1997) for individual phases but employ the median instead of the mean to improve stack coherency. Our first target is the positive velocity contrast representing the Moho of the subducted oceanic plate (Abers, 2005) because it is thought to be the largest velocity contrast and thus afford the maximum amplitude in the stacks. We use a dipping, single-layer model with mantle and crustal P velocities of 7.8 and 6.5 km/s (Ramachandran et al., 2006) to compute travel-times, although the results are only weakly dependent on this assumption (Zandt and Ammon, 1995). Travel-times are calculated from analytical solutions for a dipping interface (Frederiksen, 2001). The results at station PGC show that, on top of recovering depth and Vp/Vs from the strong positive maximum (bottom of the LVZ), we also recover the secondary, shallower and lower Vp/Vs, negative extremum from a negative velocity contrast at the top of the LVZ (Figure DR4).

DR.3. Tomography cross-sections

We show 2 cross-sections of the tomographic model along lines A1-A2 and B1-B2 (Figure 3, DR5, DR6). The positive velocity anomaly representing the thermal and compositional signature of the subducted Juan de Fuca slab extends to a depth of 300 km. The topography shown on top is exaggerated.

References

Abers, G. A., 2005, Seismic low-velocity layer at the top of subducting slabs beneath volcanic arcs: observations, predictions, and systematics: Phys. Earth Planet. Int., v. 149, p. 7-29.

Bostock, M. G., 1998, Mantle stratigraphy and architecture of the Slave craton: J. Geophys. Res., v. 103, p. 21,183-21,200.

Frederiksen, A. W., Bostock, M. G., 2001, Modelling teleseismic waves in dipping anisotropic structure: Geophys. J. Int., v. 141, p. 401-412.

Schimmel, M., Paulssen, H., 1997, Noise reduction and detection of weak, coherent signals through phase-weighted stacks: Geophys. J. Int. v. 130, p. 497–505.

Zandt, G., Ammon, C. J., 1995, Continental crust composition constrained by measurements of crustal Poisson's ratio: Nature, v. 374, p. 152–154.

Zhu, L., Kanamori, H., 2000, Moho depth variation in southern California from teleseismic receiver functions: J. Geophys. Res., v. 105, p. 2969–2980.
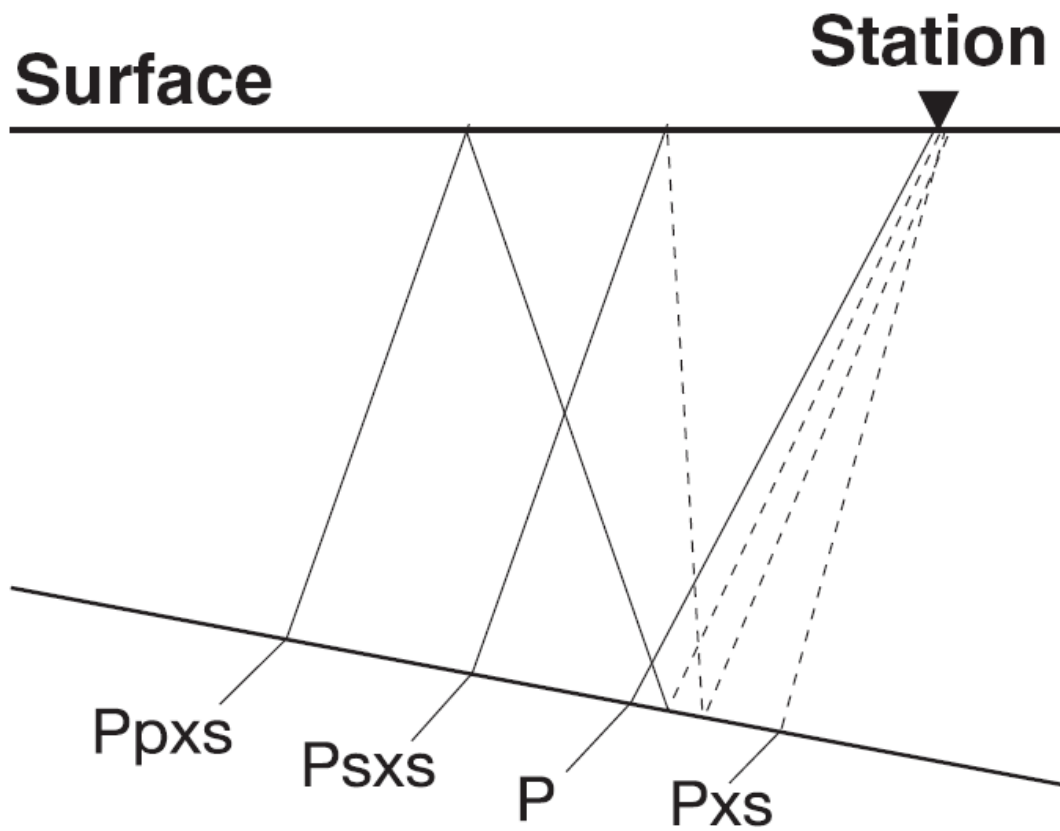
Figure DR1. Schematic illustration of P-to-S phase interactions with a dipping discontinuity identified by x. Solid lines are P waves, dashed lines are S waves. Forward conversion (Pxs) and free-surface reflections (Ppxs, Psxs) from an incident P wave. Modified from Rossi et al. (2006).
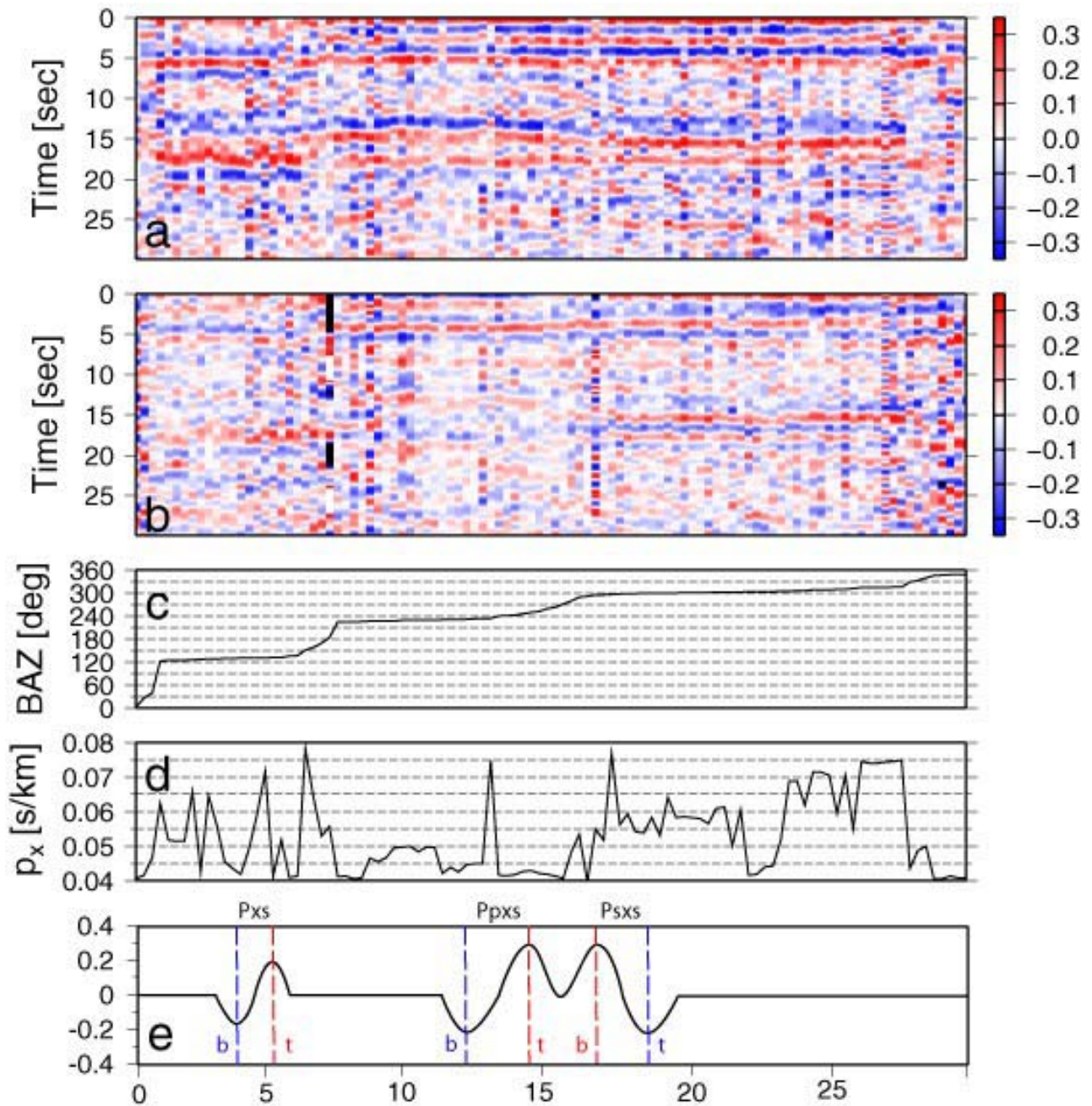
Figure DR2. Radial- (a) and transverse- (b) component receiver functions at station PGC (southern Vancouver Island) sorted by back-azimuth (c) of incident wavefields. (d) shows distribution in horizontal slowness. (e) illustrates arrivals of converted phases (Pxs, Ppxs, Psxs) from the top [t] and bottom [b] of the LVZ within the radial-component (a) receiver functions.
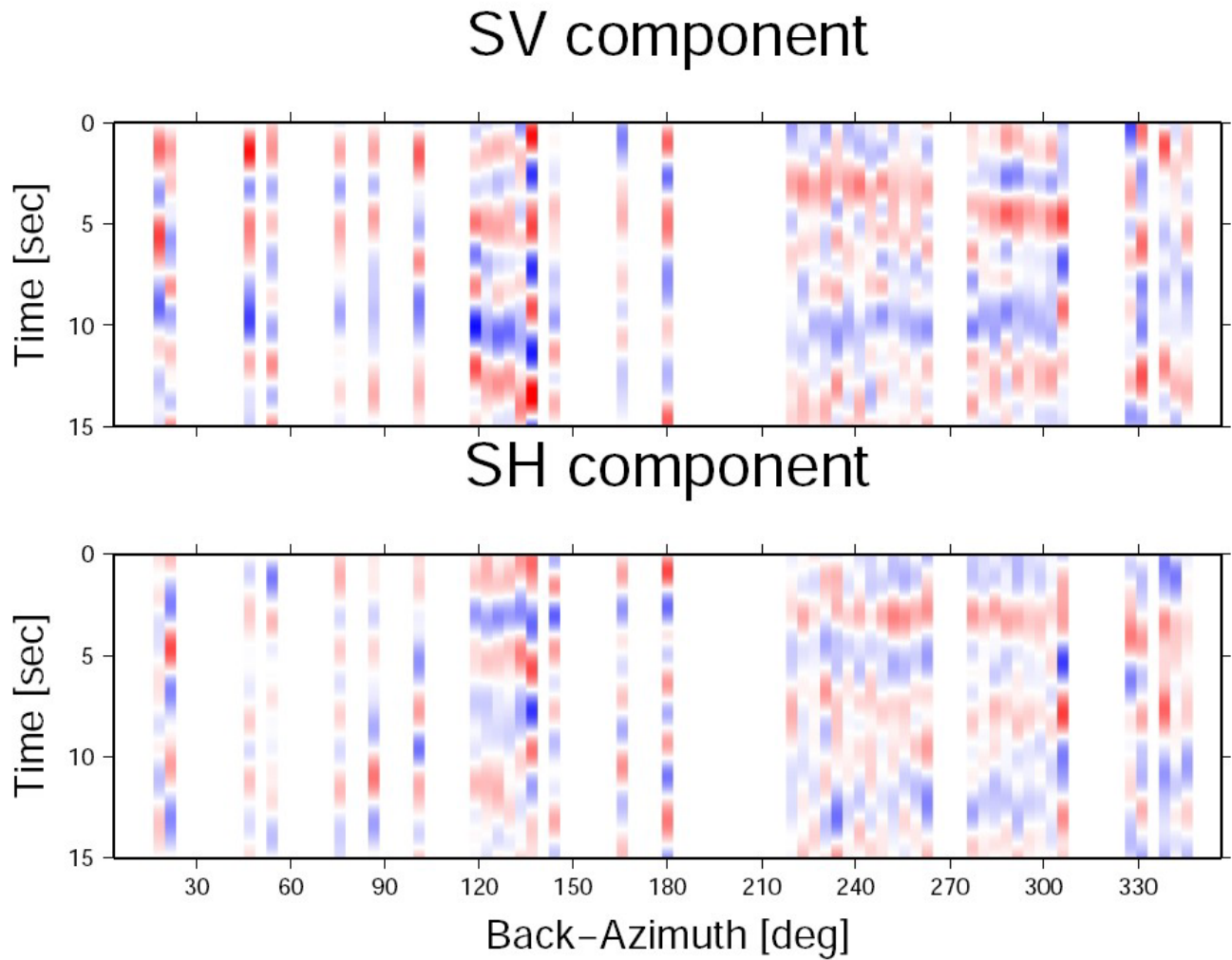
Figure DR3. Averaged radial- (SV) and transverse- (SH) component receiver functions within 10° bins for stations VI07, VI08, VI09, VI53, VI54, and WOS. One polarity reversal in Pxs signals (2-6 s) on the SV-component is clearly evident at around 270°. Polarity reversals in SH-component appear at different back-azimuths due to strike of the LVZ. SV-component Pxs signals from these stations thus manifest seismic anisotropy. We therefore give no weight to SV-component signals to avoid bias in the stacks. Color scale is the same as in Figure DR2.
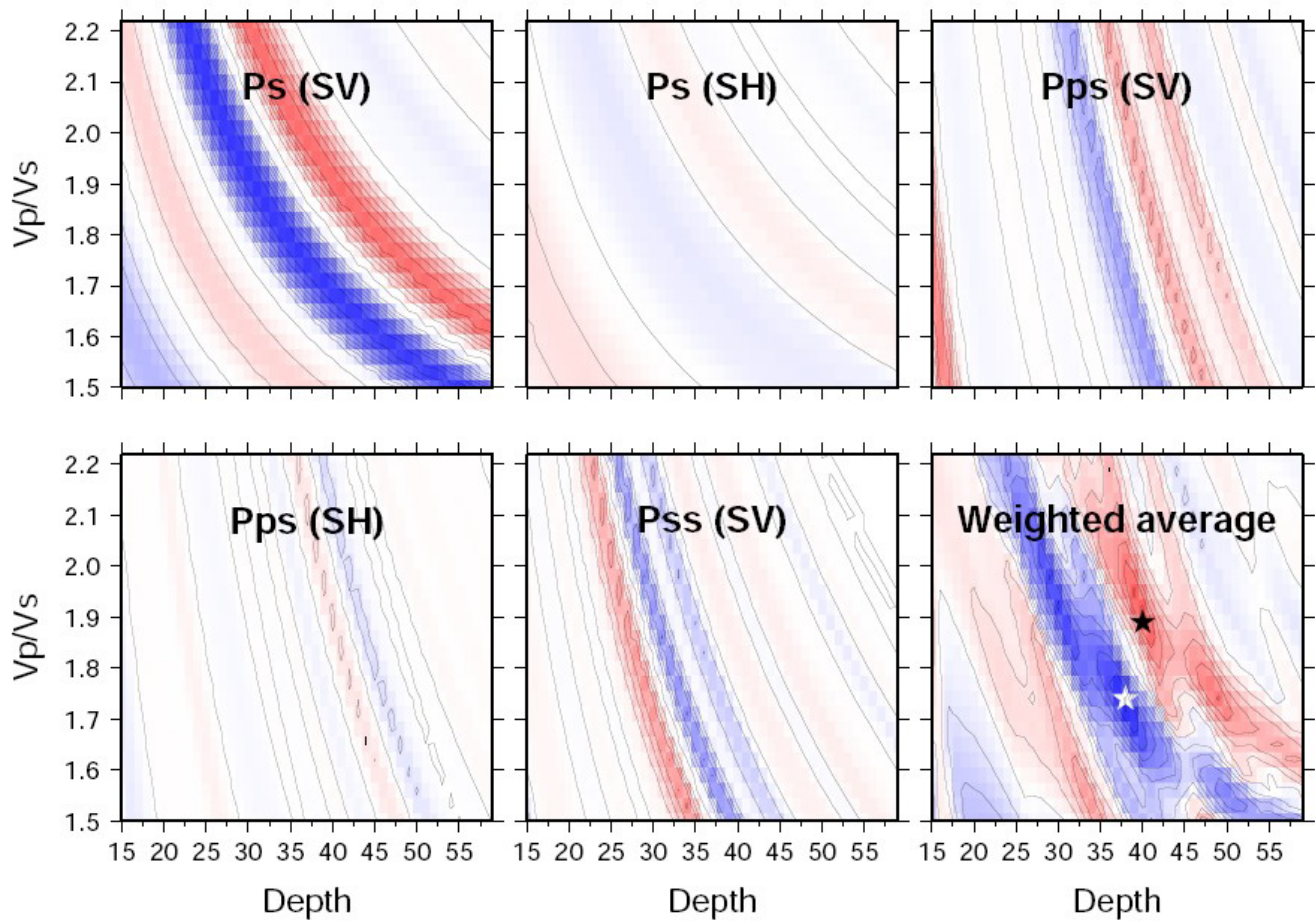
Figure DR4. Example of phase stacking for station PGC. In this case each phase is given equal weight and the moveouts are calculated for a 14° dipping discontinuity. The positive and negative extrema represent the solutions for the depth to bottom and top of the low-velocity zone, respectively, and the Vp/Vs of the overlying column.
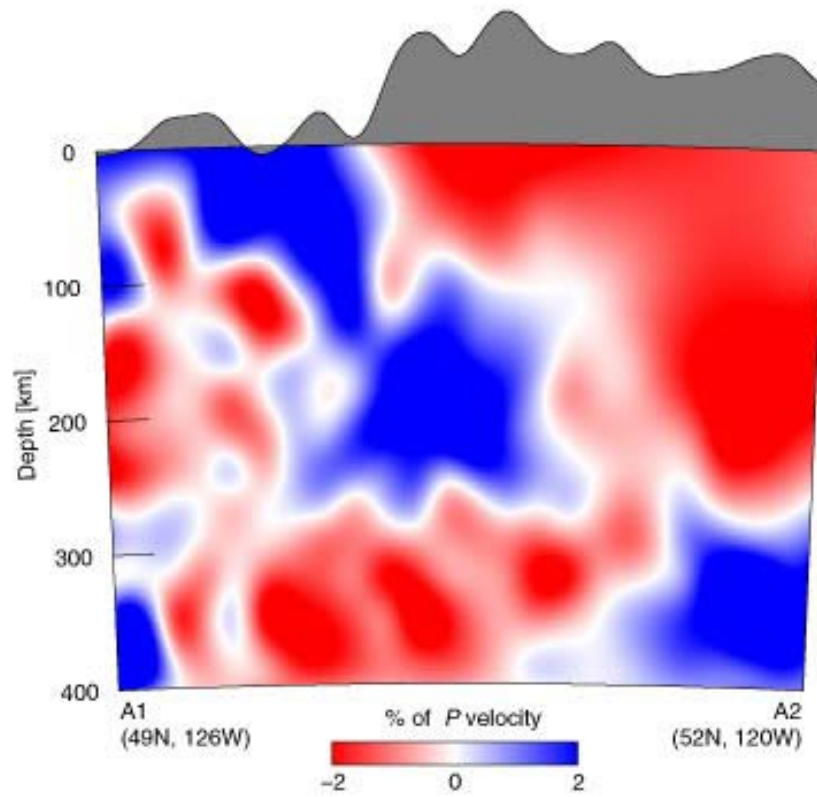
Figure DR5. Cross-section of the tomographic model along line A1-A2. The slab extends to a depth of 300 km. Its association with deeper anomalous material (positive velocity anomaly at 300-400 km) is unclear.
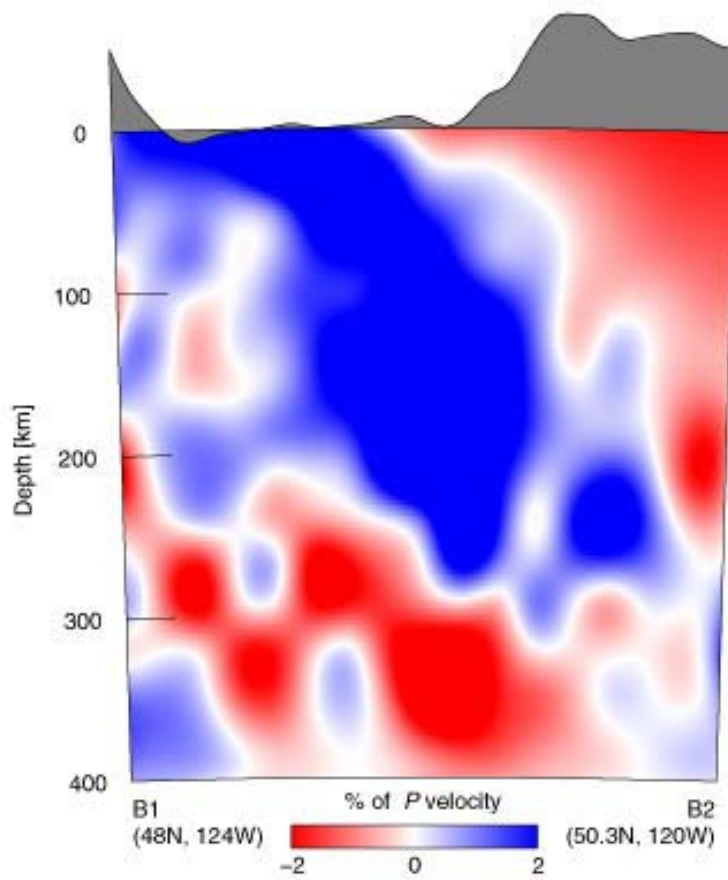
Figure DR6. Cross-section of the tomographic model along line B1-B2. The slab extends to a depth of 300 km.